New insight into the structure-property relationships from chemical bonding analysis: Application to thermoelectric materials

Hailong Yang, Pascal Boulet, Marie-Christine Record

New Insight Into the Structure-Property Relationships from Chemical Bonding Analysis: Application to Thermoelectric Materials

Hailong Yang,[a,b] Pascal Boulet [a] *, Marie-Christine Record[b]
[a] MADIREL, Aix-Marseille Université, CNRS, Marseille 13013, France
[b] IM2NP, Aix-Marseille Université, CNRS, Marseille 13013, France
* email address: pascal.boulet@univ-amu.fr

Abstract: Structure-property relationships are indisputably important to deeply understand the nature of materials. The main direction pursued to investigate these relations is based on the chemical bonding concept. The integral and local properties of chemical bonding determined from the topological analysis of electron density by combining the quantum theory of atoms in molecules (AIM) and DFT calculations can aid to build a bridge between the atomic structure and the intrinsic properties of materials. In this paper, the electronic and thermal transport properties of thermoelectric materials in the Cu-Sb-Se system have been analysed by coupling energy densities relationships and corresponding electron density Laplacian distribution for specific interactions. The asset of this method is to directly highlight the influence of lone pair electrons and atomic fluctuations on interatomic interactions as well as the coupling effect of weak bonds, which offers a new approach to design and search for materials with low thermal conductivity at low calculation cost.

Keywords: Bond theory • Density functional Theory • Electronic structure • Thermoelectrics

1. Introduction

Thermoelectricity has proved to be a promising route for harvesting wasted energy by converting heat into power. The performance of thermoelectrics is characterized by the dimensionless figure of merit, $ZT=(S^2\sigma/\kappa)T$, where S, σ, κ, and T are the Seebeck coefficient, electrical conductivity, thermal conductivity and absolute temperature, respectively. However, these parameters are severely mutually coupled, in such a way that it is hardly possible to improve one of the parameters without degrading others. In order to optimize ZT, many strategies have been developed since the 1960's, such as band-, phonon- and nano-engineering [1-4], but the understanding of the structure-properties relationships is yet insufficient to rationally design outstanding thermoelectric materials. In order to perceive the distinctions in properties between different crystal structures, various models have been developed on the basis of covalent bonding [5], dielectric constants [6] partially ionic binding [7-8] and ionicity [9]. However these models are insufficient to correctly describe the structure-property relationships. For instance, the lattice thermal conductivity (κ_L) is not only related to the ionicity of bonds [10], but also correlated to the ion coordination and vacancies [11]. Moreover, in non-normal valence compounds, both coordination and vacancies are difficult to define.

Following the discovery of abnormal interatomic distances, bond angles, large polarizability and unexpected electronic and vibrational properties of IV-VI compounds and group-V elements attributed to the resonance of bonding [12], the latter one was confirmed to have an important role in the low thermal conductivity, which results from phonon-phonon scattering [13]. The giant phonon anharmonicity in phosphorene resulting from long-range interactions also originates from the resonant bonding [14]. Recently, the analysis of low thermal conductivity of thermoelectrics has been performed by using the approach of chemical-bond hierarchy and it was shown that the phonon-phonon anharmonic scattering originates from weak chemical bonding, while the extend of weak chemical

bonds determines the lattice thermal conductivity [15-16]. This chemical approach has even been proposed for designing thermoelectric materials [17].

Trends in electronic properties and lattice thermal conductivity can be explained from electronegativity, bandwidth, orbital overlap, bond energy, bond length, and bond strength. As a consequence, the chemical approach is undoubtedly a route for developing thermoelectric materials.

Even though the required tools for analysing structure-property relationships of solids are still limited, in a previous work we analysed the chemical bonding in various systems by combining the integral with local properties of bonding [18]. This method is a simple one to characterize specific bondings in real space through density functional theory (DFT) calculations and topological analysis of the electron density on the basis of the quantum theory of atoms in molecules (QTAIM).

Since the chemical bonding is responsible for the physical and chemical properties of materials and that the bonding information can be directly obtained from the charge density, which is an observable in physics, the relationships between bonding and thermoelectric properties could be clarified by analysing the charge density of the compound of interest.

The Cu-Sb-Se ternary system is a suitable platform for analysing bonding and properties relationships since it contains three stable thermoelectric materials, namely $CuSbSe_2$, Cu_3SbSe_3 and Cu_3SbSe_4, having the same constitutive elements but discriminative thermoelectric, both electronic and thermal, properties. Cu_3SbSe_4 has a high electrical conductivity in the whole range of temperatures; Cu_3SbSe_3 has an anomalously low lattice thermal conductivity, which is almost independent of temperature; $CuSbSe_2$ has a high Seebeck coefficient in the whole range of temperatures [19-21]. In addition, Cu_4SbSe_5 and $Cu_{12}Sb_4Se_{13}$, which were predicted by theoretical studies [22], have been found as promising thermoelectric materials, in particular for $Cu_{12}Sb_4Se_{13}$, which presents an extremely low thermal conductivity. It should however be mentioned that, these compounds have never been experimentally evidenced. The $Cu_{12}Sb_4S_{13-x}Se_x$ solid solution only exists for $0<x<3$ [23].

In this paper, the investigation of structure-property relationships focusing on electronic and thermal transport, for the three existing stable compounds $CuSbSe_2$, Cu_3SbSe_3, Cu_3SbSe_4 and for the two predicted ones Cu_4SbSe_5 and $Cu_{12}Sb_4Se_{13}$ [22], hereafter named Se2, Se3, Se4, Se5 and Se13, respectively, has been performed by analysing the chemical bonding derived from the charge density.

2. Computational Methods

Density functional theory (DFT) calculations were performed using the QUANTUM ESPRESSO (QE) simulation package [24-25]. The electronic exchange-correlation energy was treated by the generalized gradient approximation (GGA) using the Perdew-Burke-Ernzerhof (PBE) [26] functionals and the interaction between ions and electrons was described by the projector augmented wave (PAW) method [27]. All the electron density was calculated with a kinetic energy cutoff for wavefunctions of 48 Ry and the Monkhorst–Pack procedure was used to generate a 4x4x4 k-points mesh for the Brillouin-zone sampling. The charge density was subsequently analyzed by the program Critic2 [28] that implements Bader's Quantum Theory of Atoms in Molecules (QTAIM) [29]. In this work, the model used in Critic2 for the kinetic energy density calculation is based on the Thomas-Fermi equation with the semiclassical gradient correction proposed by Kirzhnits [30-31]. The local energy densities of chemical bonding are interrelated by the local Virial theorem through the electron density Laplacian $\nabla^2\rho(r)$ [29],

$$\frac{1}{4}\nabla^2\rho(r) = 2G(r) + V(r) \quad (1)$$

$$G(r) + V(r) = H(r) \quad (2)$$

where G, V and H are the kinetic, potential and total energy densities, respectively. At the bond critical point (BCP) eq.(2) can be recast as:

$$\frac{H_b}{\rho_b} = \frac{G_b}{\rho_b}(1 - \frac{|V_b|}{G_b}) \quad (3)$$

Eq.(3) displays the variation of H_b/ρ_b along with $|V_b|/G_b$: the former indicator stands for the total energy per electron related to the total electronic pressure and the latter one exhibits the competition between potential energy and kinetic energy for bonding formation. These two indicators corresponding to specific characteristics of bonding can be used for the bonding classification. At the same time, the kinetic energy per electron G_b/ρ_b is related to the polarization and the rigidity of the interatomic interactions, which can reveal the bonding environment in the crystal structure [18].

In order to further investigate the long-range or weak interactions, the source function (SF) [32-34] has been used to estimate the relative contribution of an atom or group of atoms to the electron density at any point in a system, which can disclose the local and nonlocal character of the electron density distributions.

The SF, which is implemented in a modified version of Critic2 [35], is an interesting complementary tool to provide additional chemical information from the whole crystal.

In the following, the crystal structures are visualized with VESTA [36] and the figures depicting the electronic shells come directly from Critic2.

3. Results and Discussion

3.1 Electronic transport

The excellent electrical properties of Se4 are attributed to its crystal structure, consisting of the three-dimensional Cu/Se framework [Cu_3Se_4] acting as the hole conduction pathway [35]. The valence band maximum (VBM) of Se4 contains mainly a mixing of Cu-3d and Se-4p and the conduction band minimum (CBM) is dominated by the mixing of Sb-5s and Se-4p [37-38]. This Cu-3d with Se-4p mixing stabilizes holes and provides high mobility Cu/Se framework paths [37]. As the crystal structure of Se4 is tetragonal with high symmetry (space group I-42m [39], Fig.1(a)), Se4 bears one Wyckoff position for each Sb and Se atom and two ones for Cu atom. However, Cu(1)-Se and Cu(2)-Se bonds own the same distribution of $\nabla^2\rho(r)$ reported in Fig.2(a) and have almost the same bonding characteristics, as can be seen from their very close locations in Fig.3. Fig.2(a) shows that the highly delocalized valence shell charge concentration (VSCC) of Cu overlaps with the localized VSCC of Se along the bond path (BP) and this charge accumulation lies in the Se atomic basin indicating that the Cu-Se bond is a kind of ionic one. Although Fig.2(b) also shows a charge transfer in the Sb-Se bond, the VSCCs are not overlapping. Therefore the high mobility Cu/Se framework path should originate from the overlapping VSCCs between Cu and Se whereas the small void between the VSCCs of Sb and Se acts as a barrier to transport. As for Se3 and Se2, which have an orthorhombic crystal structure (space group Pnma [40-41]) as seen in Fig.1(b) and Fig.1(c), respectively, the interatomic interactions in both compounds are more complex and diverse as shown in Figure 3. By contrast to the Sb-Se interactions (see Figure 4), the Cu-Se interactions characteristics H_b/ρ_b and $|V_b|/G_b$ are not linearly dependent. The deviation from linearity originates from the severe deformation of the charge distribution between Cu and Se corresponding to the overlapped shell-structure. As exhibited in Fig.3, three kinds of Cu-Se bond exist in Se2 and a comparison between the interatomic distances of the Cu-Se bonds show that the shorter the interatomic distance the farther away from the point ($|V_b|/G_b$=1, H_b/ρ_b=0). Indeed for the bond labelled E in Fig.3, the interatomic distance is 0.03 Å larger than that of the bond labelled F. This observation is in good agreement with the fact that the ratio between the potential energy and the kinetic energy densities increases as the distance on the H_b/ρ_b vs. $|V_b|/G_b$ graph between the bond of interest and the point ($|V_b|/G_b$=1, H_b/ρ_b=0) increases. This is confirmed by the calculation of the source functions that shows a larger charge sharing magnitude as the distance to the point (1,0) increases, indicating a more local character of bonding, and a gradual VSCCs overlapping from

point A to point D in Fig.3 and Fig.5, which should lead to increasing electronic transport properties. A, B, C, D correspond to single VSCC of Cu, separate VSCCs, connected VSCCs and overlapped VSCCs, respectively. According to this analysis, the location of the Cu-Se bonds for Se5 and Se13 in Fig. 3 suggests a good electrical conductivity for these compounds, which agrees well with their semi-metallic character as reported in Ref [22], that of Se13 being less pronounced than that of Se5.

According to Yang et al. [37], the anisotropy, contributing to appropriate transport properties, in electronic and phononic transport of Se4 originates from different Cu-Se bond lengths. But the inconsistent relationship between interatomic distances and local properties of Cu-Se and Sb-Se interactions indicates that bond length only is not sufficient to evaluate the properties of bonds, especially for the bonds in semiconductors with charge transition. As a consequence the topological analysis of VSCC and local, energy density properties of bonding is the most appropriate method to explore the bonding behaviour in complex systems.

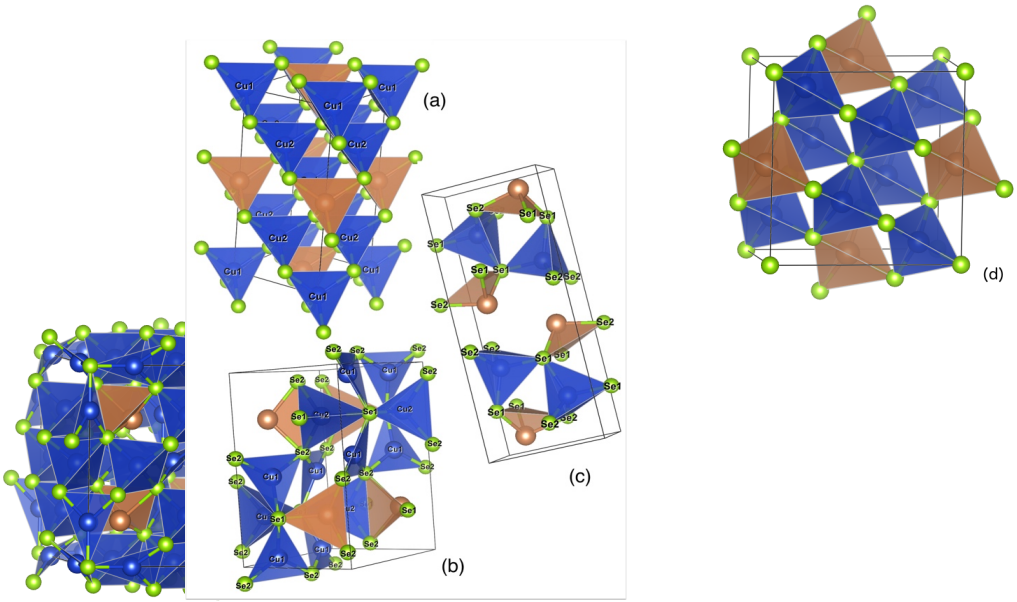

Figure 1. Crystal structures of (a) Se4, (b) Se3, (c) Se2, (d) Se5 and (e) Se13. Blue, brown and green balls stand for Cu, Sb and Se atoms, respectively.

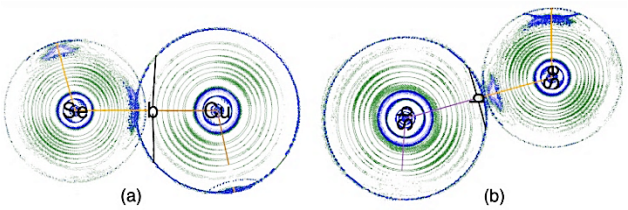

Figure 2. Electron density Laplacian of (a) Cu-Se; (b) Sb-Se in Se4. Green and blue contour curves stand for positive and negative values, respectively.

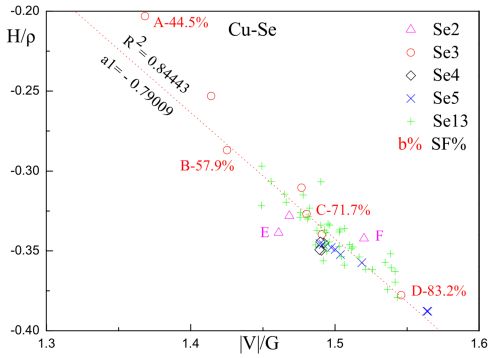

Figure 3. $|V_b|/G_b$ vs H_b/ρ_b for Cu-Se bonding of Cu-Sb-Se ternary compounds. Labels A, B, C, D, E and F stand for the different Cu-Se bonds in Se3 and Se2; the related percentage is the source contributions from directly bonded two atoms. R^2 is the regression coefficient of fitted line and a1 is its slope.

Both electronic and thermal transports are severely reduced in dispersive and non-local ionic bonds, however in Se4 there is a high similarity in bonding properties for all Cu-Se interactions as well as for all Sb-Se ones, which is the key to both electrical and thermal transport efficiency. The VSCCs analysis can explain the bonding properties but in order to compare the transport properties for different compounds we combine this analysis to the viewpoint of electronic conduction units (ECU) introduced by Bu. et al. [42].

For this, two kinds of building units are proposed in this work to describe the electronic transport in the semiconducting compounds of interest, namely one corresponding to the ionic bonds with overlapped VSCCs and the other corresponding to the ionic ones with separated VSCCs. All information on atomic interactions in Se4, Se3 and Se2 has been listed in Tab.1, Tab.2 and Tab.3, respectively. The former unit, which affords a conduction pathway, is composed by $[CuSe_4]$, $[Cu(1)Se_3]$ and $[CuSe_4]$, for Se4, Se3 and Se2 respectively, whereas the latter unit, which mostly acts as a barrier to transport, is composed by $[SbSe_4]$, $[Cu(2)Se_3]$ and $[SbSe_3]$, and $[SbSe_3]$, respectively. In Se4 the conduction pathway extends the whole crystal by means of the $[CuSe_4]$ tetrahedral units (Fig.1(a)), whereas in Se2 due to the electron confinement in the $[SbSe_3]$ units (see Fig.1(c)), the electronic transport is localized. As for Se3, the nearly planar $[Cu(1)Se_3]$ units are surrounded by $[Cu(2)Se_3]$ and $[SbSe_3]$ ones (see Fig.1(b)), leading to an even more localized transport path. These building units can explain the decrease of the electrical conductivity from Se4 to Se2 and to Se3, due to the increase in the dispersion and the delocalization of interactions, even if Cu(1)-Cu(2) metal-metal bonds are present in Se3 as shown in Fig.6(a).

In Tab.1, Tab.2 and Tab.3 the values of the kinetic energy per electron G_b/ρ_b are also reported. One can see that, the largest values of G_b/ρ_b correspond to overlapped VSCC, which can be correlated with the bond order as defined by Cremer and Kraka [43,44]. Indeed, the bond order linearly increases with G_b/ρ_b.

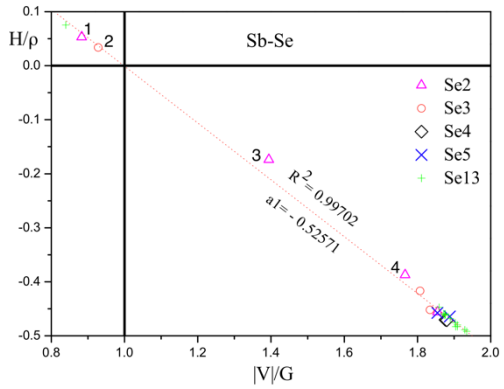

Figure 4. $|V_b|/G_b$ vs H_b/ρ_b for Sb-Se bonding in compounds of the Cu-Sb-Se system.

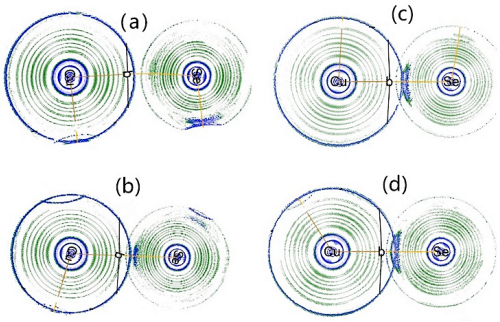

Figure 5. Electron density Laplacian of different Cu-Se bonds in Se3. (a), (b), (c) and (d) correspond to bonds labelled A, B, C, and D in Fig.3, respectively.

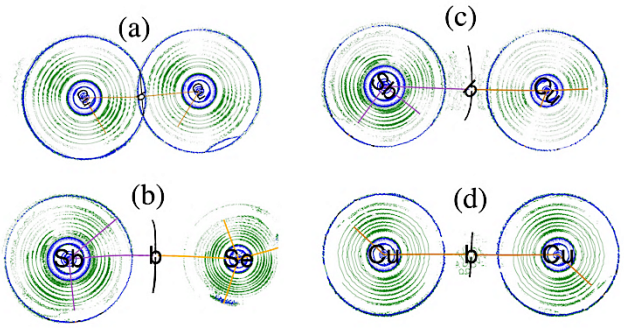

Figure 6. Electron density Laplacian of various interactions in Se3. (a) Cu-Cu metal bond; (b) Sb-Se weak interaction; (c) Sb-Cu weak interaction; (d) Cu-Cu weak interaction.

Table.1 Information on the interactions in Se4.

Atom	Interaction	No.[a]	VSCC[b]	Type	Connectivity[c]	G_b/ρ_b[d]
Cu(1)	Se	4	overlapped	ionic	4	0.70
Cu(2)	Se	4	overlapped	ionic	4	0.71
Sb	Se	4	slightly separated	ionic	4	0.54

[a] Number of interactions with adjacent atoms . [b] Main characteristic of the electron density Laplacian of specific interaction. [c] Total number of interactions for one inequivalent atom. [d] G_b/ρ_b corresponds to the kinetic energy per electron (Hartree/e).

Table.2 Information on the interactions in Se3

Atom	Interaction	No.	VSCC	Type	Connectivity	G_b/ρ_b
Cu(1)	Se(1)	1	overlapped	ionic	6	0.69
	Se(2)	2	overlapped	ionic		0.69/0.68
	Se(2)	1	single	ionic/weak		0.55
	Cu(1)	1	separated	weak		0.22
	Cu(2)	1	intersecting	metallic		0.54
Cu(2)	Se(1)	1	separated	ionic	7	0.67
	Se(1)	1	single	ionic		0.61
	Se(2)	2	separated	ionic		0.65
	Cu(1)	2	intersecting	metallic		0.54
	Sb	1	separated	weak		0.41
Sb	Se(1)	1	separated	ionic	5	0.54
	Se(1)	1	single	weak		0.47
	Se(2)	2	separated	ionic		0.52
	Cu(2)	1	separated	weak		0.41

Table.3 Information on the interactions in Se2

Atom	Interaction	No.	VSCC	Type	Connectivity	G_b/ρ_b
Cu	Se(1)	2	overlapped	ionic	4	0.73/0.66
	Se(2)	2	overlapped	ionic		0.70
Sb	Se(1)	2	separated	ionic	8	0.51
	Se(2)	1	separated	ionic		0.53
	Se(2)	2	single	weak		0.44
	Se(2)	1	single	weak		0.45
	Sb	2	separated	weak		0.47

3.2 Thermal transport

The concept of a strong vibrational mode anharmonicity induced by the presence of Sb lone-pair electrons in Se3, leading to a low thermal conductivity, is generally accepted [45-47]. This idea was originally proposed by Petrov and Shtrum [48], stating that the lone-pair 5s electrons could interact with the valence electrons of adjacent atoms upon thermal agitation, causing nonlinear repulsive forces; this nonlinearity of forces manifests itself as an anharmonicity [49]. The existence of these Sb-5s lone-pair electrons was also evidenced in Se2, indeed, it was shown that the Sb^{3+} ions were the main contributors to the averaged Grüneisen parameters [16], and that the very low thermal conductivity and distorted coordination of Se2 mainly arose from the occurrence of the lone-pair electrons of Sb as visualized by ELF [50]. As for Se4, all Sb valence electrons participated to the bonding since each Sb was tetrahedrally coordinated to Se [47], but the valence state of Sb in Se4 is still debated [38]. Actually, Skoug et al. [21] showed that in group V chalcogenides the anharmonicity extent in the crystal lattice is not only affected by the morphology of the lone-pair electron orbit but also by the coordination environment of the group V atom. However, some questions such as how the lone-pair electrons affect the atomic interactions, to what extent weak interactions can be involved in softening vibration modes and to what extent the lattice thermal conductivity can be determined by weak bonds remain unanswered. As can be seen in the following, the topological bonding analysis established in this work can help drive things forward.

The influence of lone-pair electrons on atomic interactions can be clearly seen in Fig.7. Indeed the Sb lone-pair electrons in Se3 induce two destabilized interactions ($H_b>0$) dominated by kinetic energy, namely Sb-Se(1) and Sb-Cu(2), leading to the connectivity of five with adjacent atoms. In Se2 the Sb lone-pair electrons induce two stabilized Sb-Se(2) interactions ($H_b<0$) dominated by potential energy, and one Sb-Se(2) and two Sb-Sb destabilized interactions, leading to the connectivity of eight with adjacent atoms. All these interactions have relatively low $\nabla^2\rho_b$ with a large void between VSCC and boundary of atomic basins (see Fig.6 and Fig.8 for Se3 and Se2, respectively). The atoms involved in the weak interactions play the role of “sink” with negative source contributions [34] (see Fig.9), indicating that these interactions are very strongly non-local ones with charge depletion. Moreover for a specific interaction involving the same atoms, when its characteristics at BCP is close to the ($|V_b|/G_b=1$, $H_b/\rho_b=0$) point, the non-local degree of this interaction is high. That means that for $H_b>0$, the non-local degree of the interaction increases with its strength. This behaviour is opposite to that of interactions for $H_b<0$ (see Fig.3). In this case a more local character of bonding is also observed when the distance to the point (1,0) increases but the corresponding bond strength increases. In Se2, the large contribution of the Sb atoms to the anharmonic vibrations [16] can be related to the non-local character of the weak bonds induced by the Sb-5s lone-pair electrons. Indeed the source contributions for the Sb-Sb Van der Waals interaction [42] from the adjacent four groups, namely two [$SbSe_3$] pyramids and two [$CuSe_4$] tetrahedrons, reach 80% (inset of Fig.9). This indicates a coupling between the non-local Sb-Sb weak interaction and atoms belonging to the adjacent groups, which confers to the atoms a certain extent of contribution to the anharmonic vibrations. The low atomic displacement parameter (ADP) of Sb in Se2 in comparison to that of Sb in Se3 [16] can be explained as shown in Fig.7 by the distribution of lone-pair electrons in these compounds which also agrees with the fact that lone-pair electrons in Se3 is farther removed from the Sb nucleus [21]. This dispersive distribution of lone-pair electrons in Se3 weakens both its influence on adjacent atoms and the non-local character of interatomic interactions. By contrast, in Se2 the stabilized Sb-Se interactions induced by the lone-pair electrons confine interactions between Sb and other adjacent atoms.

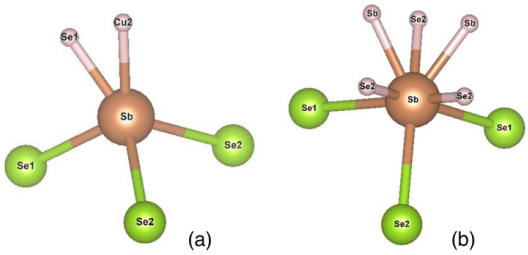

Figure.7 Connectivity of Sb in (a) Se3 and (b) Se2. Pink balls are BCPs.

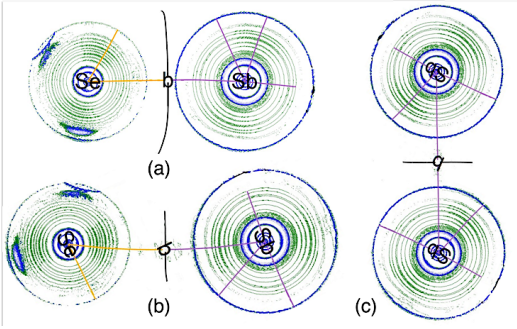

Figure 8. Electron density Laplacian of various interactions induced by lone-pair electrons in Se2. (a) Sb-Se stabilized weak interaction; (b) Sb-Se weak interaction; (c) Sb-Sb weak interaction.

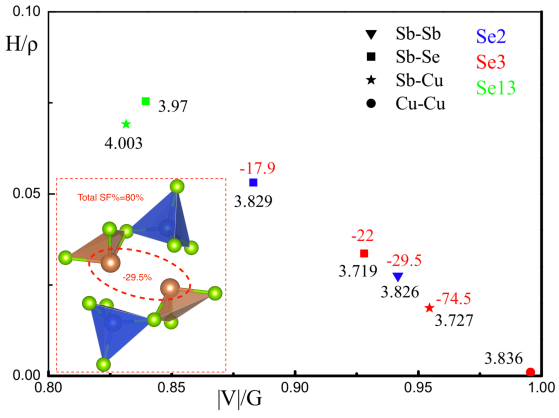

Figure 9. $|V_b|/G_b$ vs H_b/ρ_b for all destabilized interactions of Cu-Sb-Se ternary compounds. Data in red and black are the source contributions from directly bonded two atoms and interatomic distances (Å) of the corresponding interactions, respectively. The insert shows the total source contributions from adjacent groups for the Sb-Sb interaction in Se2.

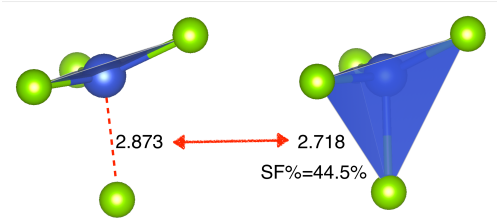

Figure 10. Vibrational motion of Cu(1) atoms in Se3. SF% is the source contributions from directly bonded atoms. The unit of interatomic distance is Å.

In addition to the weak bonds induced by Sb lone-pair electrons in Se3, other kinds of weak bonds also exist that affect the anharmonic vibrations. The out of plane motion of Cu(1) atoms induces fluctuations in the Cu(1)-Se(2) interatomic distance that goes from 2.718 Å. to 2.873 Å. (Fig.10). This Cu(1)-Se(2) interaction is a relatively weak bond, since the source contributions from directly bonded atoms involved in this interaction are 44.5% even with the shortest distance. In fact, the most important anharmonic vibrations in Se3 do not originate from Sb atoms but from Cu(1) atoms, the ADP of Cu(1) atoms being much larger than those for other species [16]. This feature is mainly attributed to the very non-local Cu(1)-Cu(1) interaction almost located at point (1,0) in Fig.9. However, the unusual temperature dependence behavior and relatively small Grüneisen parameters of all the projected acoustic phonon branches [16] indicate that intrinsic nonlinear phonon scattering is not sufficient to reach the minimal lattice thermal conductivity. Beyond the phonon-phonon anharmonic scattering, the low lattice thermal conductivity is related to phonon scattering covering relatively wide frequency range due to hierarchical chemical bonds distribution in a set of atoms coupled with each other [15]. This collective low-frequency vibration from a set of atoms is usually observed in amorphous or liquid materials, which originates from a certain group of atoms within relatively loosely packed regions that undergo a liquid-like motion from one configuration to another [51]. Qiu et al. [15-16,52] described Se3 as a part-crystalline part-liquid material with high atomic-level heterogeneity, which agrees with the above analysis. The presence of weak and non-local chemical bonding coupled with other adjacent atoms or groups of atoms (the greater the non locality of the bonding the larger the number of involved atoms) substantially widens the frequency range of phonons scattering, therefore leading to low thermal conductivity. Since in Se4 there is no weak interaction (Tab.1), the phonon-phonon scattering only occurs in a narrow range of frequencies leading to high lattice thermal conductivity. For Se3, there are two kinds of weak interactions, one originating from the Sb lone-pair electrons (Cu(2)-Sb and Sb-Se(1)), another coming from the motion of Cu(1) atoms (Cu(1)-Se(2) and Cu(1)-Cu(1)) (Tab.2).

Since these weak interactions involve all atoms in Se3, they lead to a wide range of low frequency vibrations in the crystal and thus to abnormally low lattice thermal conductivity. As for Se2, all weak interactions originate from Sb lone-pair electrons, namely Sb-Sb and Sb-Se(2) (Tab.3), and the collective low-frequency vibrations mainly arise from the groups of atoms surrounding the Sb-Sb interactions. This situation can explain a higher lattice thermal conductivity for Se2 than for Se3.

Weak bondings (H_b>0) are also observed in Se13. The location of these bonds in Fig.9 suggests a low thermal conductivity, though higher than that of Se2 and Se3 due to a lower non-local character of these bonds. This low thermal conductivity has been predicted in Ref. [22] although it has been found lower than that of Se3. The reason could be that these predictions account only for the lattice contribution to the thermal conductivity, whereas the electronic one may be substantial in semi-metal such as Se13.

3.3 Seebeck coefficient

It is reported for both Se2 and Se4 that the ionic bonding between Cu and Se atoms provide substantial DOS variation near the VBM, showing a large slope at the band edges, which leads to large Seebeck coefficient [37,50]. Furthermore, by intercalating an ionic layer, consisting of alkaline earth metals and oxygen ions, into the VDW gap of Se2, a significant enhancement of the Seebeck coefficient has been fulfilled [46]. Hence, the Seebeck coefficient has a very close-knit relationship with ionic bonding.

As seen in Tables 1, 2 and 3, all Cu-Se bonds are ionic with overlapped VSCCs in Se4 and Se2, whereas only part of Cu(1)-Se bonds in Se3 have the same features, the other ones being ionic separated or metallic.

Regarding the Sb-Se bonds, they are all ionic with separated VSCCs in Se4, separated or single VSCCs in Se3 and Se2, the number of single VSCCs being larger in Se2. In spite of the same kind of Cu-Se bonds, the Seebeck

coefficient of Se2 is higher than that of Se4, hence the difference could be due in this case to the Sb-Se bonds. It seems that the highest Seebeck coefficient is obtained when VSCC difference is well marked between Cu-Se and Sb-Se bonds, namely in Se2 where all the Cu-Se bonds are with overlapped VSCC and part of Sb-Se bonds are with single VSCC. This assumption is in agreement with the evolution of the Seebeck coefficient, which increases from Se3 to Se4 and Se2.

4. Conclusions

The structure-property relationships of materials can be analysed in the light of the topological analysis of the chemical bonding, which is sensitive to structural perturbation at atomic level. In this paper, this approach has been used to analyse electronic and thermal transport properties in thermoelectric materials. The characteristics of local energy densities for specific interactions, corresponding to the evolution of the Laplacian distribution of the electron density, are shown to be related to electrical and thermal properties of materials. By localizing the electronic transport path the dispersive and non-local ionic bonds severely affect the electrical conductivity. The asset of this approach is to directly highlight the influence of lone pair electrons and atomic fluctuations on interatomic interactions as well as the coupling effect of weak bonds. The non-locality of weak bonds determinates the extend of involved atoms, directly related to the collective frequency range of phonon scattering, which is the key to the lattice thermal conductivity of materials. This general approach based on chemical bonding analysis from the electron density is a relatively low-cost calculation one compared to that of band structure and phonon calculations, which can be easily performed as a preliminary step to design and search for materials with specific properties.

5. Acknowledgements

The authors are grateful to Pr. A. Otero de la Roza for his advices regarding technical aspects of Critic 2 program and its usage and to Pr. Tantardini for offering the C2 code implementing the source functions and the advices for its usage.

This work is financially supported by the China Scholarship Council (CSC). This work was granted access to the HPC resources of the Centre Informatique National de l'Enseignement Supérieur (CINES), Montpellier, France under allocation A0050806881 made by the Grand Equipement National de Calcul Intensif (GENCI). It was also granted access to the HPC resources of Aix-Marseille Université financed by the project Equip@Meso (ANR-10-EQPX-29-01) of the program "Investissements d'Avenir" supervised by the Agence Nationale de la Recherche.

6. References

[1] Y. Pei, X. Shi, A. LaLonde, H. Wang, L. Chen, G.J. Snyder, Convergence of electronic bands for high performance bulk thermoelectrics Nature 473 (2011) 66-69. https://doi.org/10.1038/nature09996.

[2] W. Kim, Strategies for engineering phonon transport in thermoelectrics, J. Mater. Chem. C 3 (2015) 10336-10348. https://doi.org/10.1039/C5TC01670C.

[3] Z. Chen, X. Zhang, Y. Pei, 2018. Manipulation of Phonon Transport in Thermoelectrics, Adv. Mater. 30, 1705617. https://doi.org/10.1002/adma.201705617.

[4] S. R. Boona, Nanomagnets boost thermoelectric output, Nature 549 (2017) 169-170. https://doi.org/10.1038/549169a.

[5] J. C. Phillips, A Posteriori Theory of Covalent Bonding, Phys. Rev. Lett. 19 (1967), 415-417. https://doi.org/10.1103/PhysRevLett.19.415.

[6] J. C. Phillips, Dielectric Definition of Electronegativity, Phys. Rev. Lett. 20 (1968), 550-553. https://doi.org/10.1103/PhysRevLett.20.550.

[7] J. C. Phillips, Covalent Bond in Crystals. II. Partially Ionic Binding, Phys. Rev. 168 (1968) 905-911. https://doi.org/10.1103/PhysRev.168.905.

[8] J. C. Phillips, J. A. Van Vechten, Dielectric Classification of Crystal Structures, Ionization Potentials, and Band Structures, Phys. Rev. Lett. 22 (1969), 705-708. https://doi.org/10.1103/PhysRevLett.22.705.

[9] P. J. Stiles, Trends in the ionicity in the average valence V materials, Solid State Commun. 11 (1972**)**, 1063-1066. https://doi.org/10.1016/0038-1098(72)90321-3.

[10] A. V. Ioffe, A. F. Ioffe, Thermal conductivity of semiconductor solid solutions, Sov. Phys. - Sol. State 2 (1960) 719-728.

[11] D. P. Spitzer, Lattice thermal conductivity of semiconductors: A chemical bond approach, J. Phys. Chem. Solids 31 (1970) 19-40. https://doi.org/10.1016/0022-3697(70)90284-2.

[12] G. Lucovsky, R. M. White, Effects of Resonance Bonding on the Properties of Crystalline and Amorphous Semiconductors, Phys. Rev. B 8 (1973) 660-667. https://doi.org/10.1103/PhysRevB.8.660.

[13] S. Lee, K. Esfarjani, T. Luo, J. Zhou, Z. Tian & G. Chen, 2014. Resonant bonding leads to low lattice thermal conductivity, Nat. Commun. 5, 3525. https://doi.org/10.1038/ncomms4525.

[14] G. Qin, X. Zhang, S. Y. Yue, Z. Qin, H. Wang, Y. Han, M. Hu, 2016. Resonant bonding driven giant phonon anharmonicity and low thermal conductivity of phosphorene, Phys. Rev. B 94, 165445. https://doi.org/10.1103/PhysRevB.94.165445.

[15] W. Qiu, L. Xi, P. Wei, X. Ke, J. Yang, and W. Zhang, Part-crystalline part-liquid state and rattling-like thermal damping in materials with chemical-bond hierarchy, Proc. Natl. Acad. Sci. U.S.A. 111 (2014) 15031-15035. https://doi.org/10.1073/pnas.1410349111.

[16] W. Qiu, L. Wu, X. Ke, J. Yang, W. Zhang, 2015. Diverse lattice dynamics in ternary Cu-Sb-Se compounds, Sci. Rep. 5, 13643. https://doi.org/10.1038/srep13643.

[17] W. G. Zeier, A. Zevalkink, Z. M. Gibbs, G. Hautier, M.G. Kanatzidis, G.J. Snyder, Thinking Like a Chemist: Intuition in Thermoelectric Materials, Angew. Chem. Int. Ed. 55 (2016), 6826-6841. https://doi.org/10.1002/anie.201508381.

[18] H. L. Yang, M.-C. Record, P. Boulet, A rapid method for analyzing the chemical bond from energy densities calculations at the bond critical point, submitted to *Computational and Theoretical Chemistry* on January 8th, 2020.

[19] E. J. Skoug, J. D. Cain, D. T. Morelli, 2011. High thermoelectric figure of merit in the Cu_3SbSe_4-Cu_3SbS_4 solid solution , Appl. Phys. Lett. 98, 261911. https://doi.org/10.1063/1.3605246.

[20] E. J. Skoug, J. D. Cain, D. T. Morelli, M. Kirkham, P. Majsztrik, and E. Lara-Curzio, 2011. Lattice thermal conductivity of the Cu3SbSe4-Cu3SbS4 solid solution, J. Appl. Phys. 110, 023501. https://doi.org/10.1063/1.3610385.

[21] E. J. Skoug, D. T. Morelli, 2011. Role of lone-pair electrons in producing minimum thermal conductivity in nitrogen-group chalcogenide compounds. Phys. Rev. Lett. 107, 235901. https://doi.org/10.1103/PhysRevLett.107.235901.

[22] Y. Zhang, V. Ozolins, D. Morelli, C. Wolverton, Prediction of new stable compounds and promising thermoelectrics in the Cu–Sb–Se system. Chem. Mater. 26 (2014) 3427-3435. https://doi.org/10.1021/cm5006828.

[23] X. Lu, D. T. Morelli, Y. Wang, W. Lai, Y. Xia, V. Ozoliņš, Phase Stability, Crystal Structure, and Thermoelectric Properties of $Cu_{12}Sb_4S_{13-x}Se_x$ Solid Solutions, Chem. Mater. 28 (2016) 1781-1786.

[24] P. Giannozzi, S. Baroni, N. Bonini, M. Calandra, R. Car, C. Cavazzoni, D. Ceresoli, G.L. Chiarotti, M. Cococcioni, I. Dabo, 2009. QUANTUM ESPRESSO: a modular and open-source software project for quantum simulations of materials, J. Phys.: Condens. Matter, 21, 395502.

[25] P. Giannozzi, O. Andreussi, T. Brumme, O. Bunau, M.B. Nardelli, M. Calandra, R. Car, C. Cavazzoni, D. Ceresoli, M. Cococcioni, N. Colonna, I. Carnimeo, A. Dal Corso, S. de Gironcoli, P. Delugas, R. A. DiStasio Jr, A. Ferretti, A. Floris, G. Fratesi, G. Fugallo, R. Gebauer, U. Gerstmann, F. Giustino, T. Gorni, J. Jia, M. Kawamura, H.-Y. Ko, A. Kokalj, E. Küçükbenli, M. Lazzeri, M. Marsili, N. Marzari, F. Mauri, N.L. Nguyen, H.-V. Nguyen, A. Otero-de-la-Roza, L. Paulatto, S. Poncé, D. Rocca, R. Sabatini, B. Santra, M. Schlipf, A.P. Seitsonen, A. Smogunov, I. Timrov, T. Thonhauser, P. Umari, N. Vast, X. Wu and S. Baroni, 2017. Advanced capabilities for materials modelling with Quantum ESPRESSO, J. Phys.: Condens. Matter, 29, 465901. https://doi.org/10.1088/1361-648X/aa8f79.

[26] J. P. Perdew, K. Burke, M. Ernzerhof, Generalized Gradient Approximation Made Simple, Phys. Rev. Lett. 77 (1996), 3865-3868. https://doi.org/10.1103/PhysRevLett.77.3865.

[27] P. E. Blöchl, Projector augmented-wave method, Phys. Rev. B 50 (1994) 17953-17979. https://doi.org/10.1103/PhysRevB.50.17953.

[28] A. Otero-de-la-Roza, E. R. Johnson, V. Luaña, Critic2: A program for real-space analysis of quantum chemical interactions in solids, Comput. Phys. Commun. *185 (*2014), 1007-1018. https://doi.org/10.1016/j.cpc.2013.10.026.

[29] R.F.W. Bader, *Atoms in Molecules: A Quantum Theory*, Oxford University Press, 1990.

[30] D.A. Kirzhnits, Quantum corrections to the Thomas-Fermi equation, Sov. Phys. – J. Exp. Theor. Phys.**,** 5 (1957) 64-71.

[31] D.A. Kirzhnits, Field Theoretical Methods in Many-Body Systems, Pergamon Press, Long Island City, N.Y., 1967.

[32] R.F.W. Bader, C. Gatti, A Green's function for the density, Chem. Phys. Lett., 287 (1998) 233-238. https://doi.org/10.1016/S0009-2614(97)01457-7.

[33] C. Gatti, F. Cargnoni, L. Bertini, Chemical information from the source function, J. Comput. Chem., 24 (2003), 422-436. https://doi.org/10.1002/jcc.10205.

[34] C. Gatti, D. Lasi, Source function description of metal–metal bonding in d-block organometallic compounds, Faraday Discussions, 135 (2007), 55-78. https://doi.org/10.1039/B605404H.

[35] C. Tantardini, D. Ceresoli, E. Benassi, Source function and plane waves: Toward complete bader analysis, J. Comput. Chem., 37 (2016), 2133-2139. https://doi.org/10.1002/jcc.24433.

[36] K. Momma, F. Izumi, VESTA 3 for three-dimensional visualization of crystal, volumetric and morphology data, *J. Appl. Crystallogr.*, 44, 1272-1276 (2011).

[37] C. Yang, F. Huang, L. Wu, K. Xu, 2011. New stannite-like p-type thermoelectric material Cu_3SbSe_4, J. Phys. D: Appl. Phys. 44, 295404. https://doi.org/10.1088/0022-3727/44/29/295404.

[38] D. Do, V. Ozolins, S. D. Mahanti, et al., 2012. Physics of bandgap formation in Cu–Sb–Se based novel thermoelectrics: the role of Sb valency and Cu d levels, J. Phys.: Condens. Matter, 24, 415502. https://doi.org/10.1088/0953-8984/24/41/415502

[39] A. Pfitzner, Crystal structure of tricopper tetraselenoantimonate (V), Cu_3SbSe_4, Z. Kristallogr. Cryst. Mater. 209 (1994) 685-685. https://doi.org/10.1524/zkri.1994.209.8.685.

[40] A. Pfitzner, Cu_3SbSe_3: Synthese und Kristallstruktur, Z. Anorg. Allg. Chem. 621 (1995), 685-688. https://doi.org/10.1002/zaac.19956210431.

[41] R.M. Imamov, Z.G. Pinsker, Determination of crystal structure of CuSbSe, Sov. Phys. Crystallogr. 9 (1965), 721-723.

[42] K. Bu, J. Huang, M. Luo, M. Guan, C. Zheng, J. Pan, X. Zhang, S. Wang, W. Zhao, X. Shi, L. Xu, F. Huang, Observation of High Seebeck Coefficient and Low Thermal Conductivity in [SrO]-Intercalated $CuSbSe_2$, Compound Chem. Mater. 30 (2018), 5539-5543. https://doi.org/10.1021/acs.chemmater.8b02651.

[43] D. Cremer, E. Kraka, Chemical Bonds without Bonding Electron Density? Does the Difference Electron-Density Analysis Suffice for a Description of the Chemical Bond?, Angew. Chem. Int. Ed. 23 (1984) 627-628.

[44] D. Cremer, E. Kraka, A Description of the Chemical Bond in Terms of Local Properties of Electron Density and Energy, Croatica Chem. Acta 57 (1984) 1259-1281.

[45] K. Tyagi, B. Gahtori, S. Bathula, A.K. Srivastava, A.K. Shukla, S. Auluck, A. Dhar, Thermoelectric properties of Cu_3SbSe_3 with intrinsically ultralow lattice thermal conductivity, J. Mater. Chem. A 2 (2014), 15829-15835. https://doi.org/10.1039/C4TA02590C.

[46] E. J. Skoug, J. D. Cain, D. T. Morelli, 2010. Structural effects on the lattice thermal conductivity of ternary antimony- and bismuth-containing chalcogenide semiconductors, Appl. Phys. Lett. 96, 181905. https://doi.org/10.1063/1.3425886.

[47] Y. Zhang, E. Skoug, J. Cain, V. Ozoliņš, D. Morelli, C. Wolverton, 2012. First-principles description of anomalously low lattice thermal conductivity in thermoelectric Cu-Sb-Se ternary semiconductors, Phys. Rev. B, 85, 054306. https://doi.org/10.1103/PhysRevB.85.054306.

[48] A.V. Petrov, E.L. Shtrum, Heat Conductivity and the Chemical Bond in ABX2-Type Compounds, Sov. Phys. - Sol. State 4 (1962), 1061-1065.

[49] D. T. Morelli, V. Jovovic, J. P. Heremans, 2008. Intrinsically Minimal Thermal Conductivity in Cubic I−V−VI_2 Semiconductors, Phys. Rev. Lett. 101, 035901. https://doi.org/10.1103/PhysRevLett.101.035901.

[50] D. Zhang, J. Yang, Q. Jiang, L. Fu, Y. Xiao , Y. Luo, Z. Zhou, Ternary $CuSbSe_2$ chalcostibite: facile synthesis, electronic-structure and thermoelectric performance enhancement, J. Mater. Chem. A 4 (2016), 4188-4193. https://doi.org/10.1039/C6TA00039H.

[51] W.H. Wang, Roles of minor additions in formation and properties of bulk metallic glasses, Prog. Mater. Sci. 52 (2007), 540-596. https://doi.org/10.1016/j.pmatsci.2006.07.003.

[52] W.J. Qiu, X.Z. Ke, L.L. Xi, L. Wu, J. Yang, W. Zhang, 2016. “Phonon” scattering beyond perturbation theory, Science China Phys. Mech. Astron., 59, 627001. https://doi.org/10.1007/s11433-015-5769-1.